Co-electrolysis of Biohythane using Solid Oxide Fuel Cell Technology

K. Panagi[a], C. J. Laycock[a], J. P. Reed[a], A. J. Guwy[a]

[a] Sustainable Environment Research Centre, University of South Wales, Pontypridd, CF37 4BD, United Kingdom

Two-stage anaerobic digestion enables the production of biohythane, which is composed of 60/30/10 vol% $CH_4/CO_2/H_2$ and is easier and more beneficial to utilize than conventional biogas (60/40 vol% CH_4/CO_2). This study has investigated co-electrolysis of biohythane with H_2O and CO_2 using an anode-supported solid oxide fuel cell. The kinetic performance of the cell was characterized using I-V curves and electrochemical impedance spectroscopy. The output gases from the anode were characterized using quadrupole mass spectrometry. The work has shown that addition of 10 vol% H_2 to CH_4/CO_2 feedstocks markedly improves the overall performance of the cell in electrolysis mode. Co-electrolyzing with H_2O gave the highest performance, highest syngas (H_2 + CO) yield (87%) and highest H_2/CO ratio (2.69). Co-electrolyzing with CO_2 decreased the catalytic and electrochemical conversion of reactants, giving lower performance, lower syngas yields (79%) and lower H_2/CO ratios (0.87). Enhanced performance with H_2O was due to a mixture of increased catalytic and electrochemical conversion of reactants.

Introduction

Anaerobic digestion (AD) is an established and widely deployed technology that enables the production of useful feedstocks from food and organic wastes (1). The process of AD involves bacterial digestion of organic materials in the absence of oxygen, and takes place in four stages: 1) hydrolysis, 2) acidogenesis, 3) acetogenesis, and 4) methanogenesis (2-3). In stages 1-2, the waste substrate is converted into a gaseous 50/50 vol% H_2/CO_2 mixture known as biohydrogen. A liquid phase rich in short-chain C1-C5 carboxylic acids and alcohols is also produced. In stage three, the H_2 and CO_2 are converted into carboxylic acids, which are converted in stage four by methane producing bacteria into a gaseous 60/40 vol% CH_4/CO_2 mixture (known as biogas) and a liquid phase digestate rich in nutrients. AD processes where all four stages are carried out in one reactor is referred to as single-stage fermentation (4).

It is possible to achieve increased energetic gains by carrying out stages one and two in a separate reactor to stages three and four (5-10). This is known as two-stage fermentation and enables each of the stages to be optimized separately. The biohydrogen (H_2/CO_2) and biogas (CH_4/CO_2) produced from each reactor can then be combined to produce a biohythane mixture typically composed of 60/30/10 vol% $CH_4/CO_2/H_2$. This potentially results in a 37% greater energy yield compared with single-stage AD (5-10).

Furthermore, the additional presence of H_2 makes biohythane easier and more beneficial to utilize than conventional methane-rich biogas (5-10).

There has been very little previous work into the utilization of biohythane in SOFC technology. The most relevant work has investigated the utilization of $CH_4/CO_2/H_2$ mixtures in fuel cell mode, and has indicated that fuel utilization takes place through a mixture of catalytic and electrochemical processes (11-14). Electrochemical conversion of fuels predominantly takes place via electrochemical H_2 oxidation [1], which has considerably lower activation losses than CH_4 oxidation [2]:

$$H_2 + O^{2-} \rightleftharpoons H_2O + 2e^- \quad [1]$$

$$CH_4 + O^{2-} \rightleftharpoons 2H_2O + CO_2 + 8e^- \quad [2]$$

A key issue with utilizing $CH_4/CO_2/H_2$ mixtures in SOFC technology is the very slow kinetics of CH_4 oxidation compared with those of H_2-based fuels. In addition, anode oxidation and methane cracking [3] decrease cell performance and deactivate the anode over longer time durations (12):

$$CH_4 \rightleftharpoons 2H_2 + C \quad [3]$$

Catalytic dry reforming of methane [4] and the reverse water-gas shift (RWGS) reaction [5] have a major role in the conversion of $CH_4/CO_2/H_2$ mixtures and the subsequent performance of the cell:

$$CH_4 + CO_2 \rightleftharpoons 2H_2 + 2CO \quad [4]$$

$$H_2 + CO_2 \rightleftharpoons H_2O + CO \quad [5]$$

In particular, dry reforming of CH_4 increases cell performance by increasing the open circuit potential (OCP) and decreasing the electrochemical CH_4 oxidation activation losses. These processes can also alleviate problems caused by anode oxidation and methane cracking (13-14).

This paper investigates the utilization of simulated biohythane mixtures in an anode-supported solid oxide fuel cell (SOFC) by co-electrolyzing with H_2O, CO_2 and H_2O/CO_2 oxidant mixtures. The kinetic performance of the cell has been characterized using I-V curves and electrochemical impedance spectroscopy. The performance of the cell was compared with H_2 as well as biohydrogen and biogas. The performance and gaseous outputs of the cell were measured and compared for each of the three oxidant mixtures, providing insights into the mechanism of fuel conversion at the anode. The kinetic performance of the cell was characterized using I-V curves and electrochemical impedance spectroscopy. The output gases from the anode were characterized in real-time using quadrupole mass spectrometry (QMS), showing the gaseous products and transient behavior of fuel conversion in a high level of detail.

Experimental

All measurements and testing were carried out at 750 °C using a commercially available anode-supported cell (ASC) (FCM, ASC-2.0, 213308). The cell was composed of a 3 μm 8-yttria-stablised zirconia (8-YSZ) electrolyte layer, a 3 μm gadolinia-doped ceria (GDC) barrier layer, a 400 μm NiO-YSZ anode electrode support and a 12 μm lanthanum strontium chromite (LSC) cathode. The diameter of the anode and electrolyte layers was 20 mm and the diameter of the cathode was 12.5 mm.

Mounting and Conditioning of the ASC

The cell was tested using a Fiaxell Open Flanges SOFC test set-up. Detailed information on the test set-up is available on the Fiaxell website (15). The ASC was mounted within two spring-loaded flanges on the underside of the test set-up. The flanges were made with Inconel 600 and 601 and enabled feeding of air and fuel gases to the cell. A gas-tight seal preventing fuel and oxidant crossover was created by pressing the cell between two sheets of alumina felt within the flanges. Electrical current collection wires were also positioned within the alumina felt sheets. Gold wire mesh and nickel foam were used for current collection at the cathode and anode respectively. The temperature of the cell was measured using a type-K thermocouple, which was positioned above the cell on top of the alumina felt. The cell, wires, nickel foam and thermocouple were held in position during mounting using silica-free tape and adhesive. The flanges were then spring loaded, completing the cell mounting procedure.

Once mounted, the underside of the test set-up was placed within a chamber furnace which was used to heat the cell to the required temperature. The current collection and voltage sensing wires were connected to a potentiostat (Ivium Technologies IviumStat), enabling electrochemical measurements to be carried out. Gas delivery and recovery connections were made using stainless steel Swagelok fittings. Air (Air Liquide, 99.99%) was supplied to the cathode using a rotameter. Fuel gases were supplied to the anode using a Bronkhorst Flow-SMS digital mass flow controller system, which enabled the delivery of gaseous mixtures containing CH_4 (Air Liquide, 99.5%)), Air (Air Liquide, 99.99%), H_2 (Air Liquide, 99.999%), CO_2 (Air Liquide, 99.99%) and He (Air Liquide, 99.999%). Fuel mixtures were mixed with steam using an integrated ceramic cartridge containing alumina fibers. Deionized water was delivered through the cartridge using a peristaltic pump at the required flow rate. The cartridge was resistively heated from the chamber furnace, enabling a constant steam flux to be delivered to the anode as required. Product gases from the anode were collected continuously and fed into a quadrupole mass spectrometer (MKS Instruments), enabling continuous measurement of the product gas composition.

The test set-up was initially heated at 120 °C h^{-1} up to 400 °C, followed by a second heating ramp of 200 °C h^{-1} up to 750 °C. During initial heating, air was supplied at 100 cm^3 min^{-1} to the cathode in order to burn off the tape and adhesive used during cell mounting and 30 cm^3 min^{-1} of helium was supplied to the anode. When the cell reached 750 °C, the spring-loaded pressure of the flanges was checked and corrected as required. 5 vol% H_2 was then added to the mixture in order to reduce the anode and nickel foam, which was monitored by observing the OCP of the cell. When the OCP had stabilized,

the H_2 content was increased to 10 vol% until the OCP had re-stabilized. This procedure was repeated until the gas stream consisted of pure H_2. The OCP observed under pure H_2 was 1.13 V at 750 °C, indicating negligible gas crossover and current loss. Finally, a voltage of 0.8 V was applied to the cell for 24 hours in order to condition the electrolyte.

Electrochemical Measurements

The electrochemical performance of the cell was studied in electrolysis mode running on fuel mixtures containing CH_4, CO_2, H_2 and H_2O as required. Each fuel mixture was supplied at a flow rate of 30 cm^3 min^{-1}. For mixtures containing CH_4, air was added to give a CH_4/air ratio of 5:1 by volume in order to prevent any interference to data caused by carbon deposition. For all fuels studied, the complete gas mixture was balanced in He in order to give a consistent total fuel gas flow rate of 36 cm^3 min^{-1}. Upon changing fuel mixtures, the cell was left to stabilize for 30 minutes before collecting data. 50 cm^3 min^{-1} of air was supplied to the cathode for all measurements taken. Current-voltage (I-V) curves were measured over the range OCP - 2 V at a scan rate of 50 mV s^{-1}. Electrochemical impedance spectroscopy (EIS) measurements were taken potentiostatically over the frequency range 0.1 kHz - 100 MHz using a voltage amplitude of 10 mV. EIS measurements were carried out in electrolysis mode at 0.1 V above the OCP.

Anode Output Gas Analysis using Quadrupole Mass Spectrometry

The composition of the output gases leaving the anode was measured using QMS. The spectrometer was primarily set to measure the intensities of m/z = 2 (H_2), 15 (CH_4), 28 (CO), and 44 (CO_2). The sensitivity of the spectrometer towards each of the gases was measured and used for data correction, so that the data presented in this work represents the relative partial pressures of the output gases leaving the cell. He (m/z = 4) was used as the carrier gas. When taking QMS measurements, fuel gases were delivered at a rate of 8 cm^3 min^{-1} and diluted in 22 cm^3 min^{-1} of He to give a total gas flow rate to the cell of 30 cm^3 min^{-1}. It was necessary to remove H_2O present in the output gases using a silica gel desiccant in order to prevent water collection issues within the QMS. The presence of H_2O in the output gases was therefore not measured.

Results and Discussion

Firstly, the ASC was operated in electrolysis mode using a 50/50 vol% H_2/H_2O mixture. Table I shows the OCP was 0.948 V and Fig. 1 shows the I-V curve was linear up to approx. 1.2 V, indicating the activation and concentration losses were very low. Adding 50 vol% CO_2 to the fuel (still mixed with 50 vol% H_2O in total) decreased the OCP to 0.925 V which, based on results from previous work (16-18), was due to CO_2 dilution effects and the presence of the RWGS reaction, which further decreased the presence of H_2 and generated CO at the anode. The I-V curve was very similar to that measured for pure H_2, showing the CO_2 had very little effect on the activation and concentration losses of the cell.

Switching the fuel from biohydrogen to 60/40 vol% CH_4/CO_2 biogas caused the cell performance to deteriorate. The OCP increased to 1.016 V in agreement with previous work due to the presence of dry [4] and steam [6] reforming of CH_4, which both increased the volume of H_2 at the anode:

$$CH_4 + H_2O \rightleftharpoons 3H_2 + CO \qquad [6]$$

In addition, the overall kinetic performance decreased due to a considerable increase in the activation losses as indicated by the pronounced curve across the full voltage range.

These losses were alleviated slightly by switching to biohythane (60/30/10 vol% $CH_4/CO_2/H_2$), which gave a similar I-V curve but with decreased activation losses compared with biogas, showing that even adding only 10 vol% H_2 to the fuel mixture improved the kinetic performance of the cell: for example, a voltage approx. 17% lower was required to achieve 400 mA cm^{-2}. Adding H_2 also resulted in a lower OCP than biogas, suggesting that H_2 suppressed catalytic reforming reactions at the anode. The enhanced performance overall compared with biogas is most likely due to improved reduction of the anode surface and suppression of methane cracking, thereby promoting catalytic conversion of CH_4 through dry reforming (19-21).

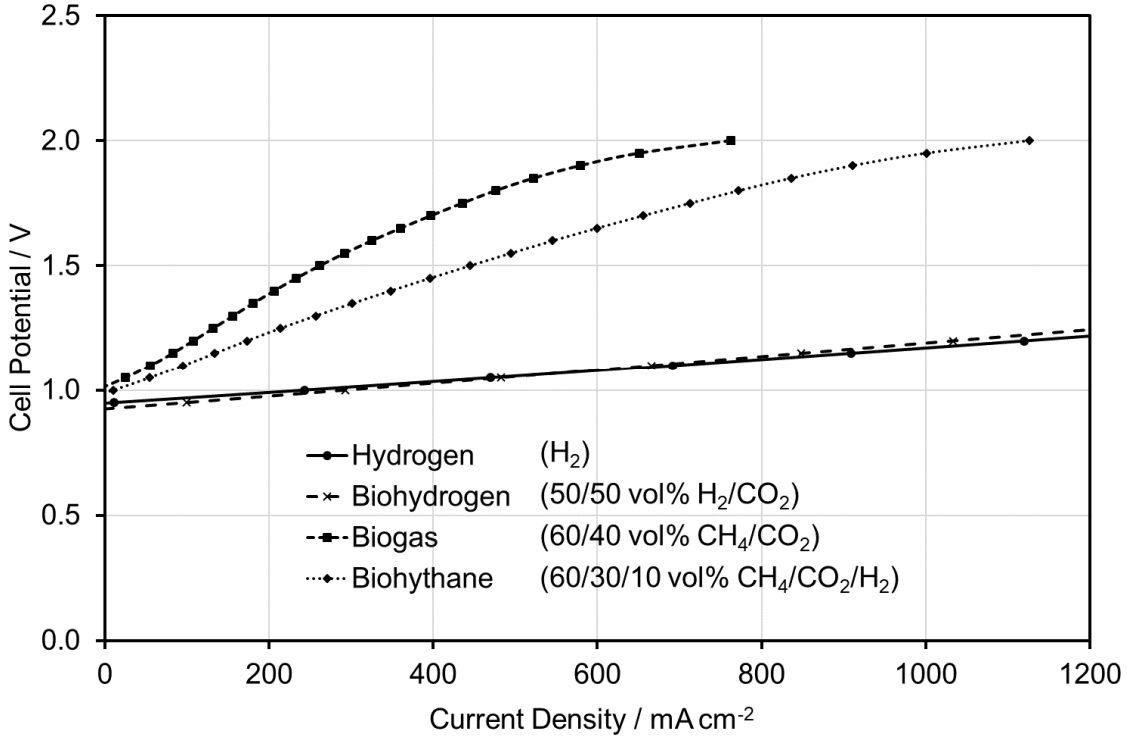

Figure 1. I-V curves of an ASC operating on hydrogen (H_2), biohydrogen (50/50 vol% H_2/CO_2), biogas (60/40 vol% CH_4/CO_2) and biohythane (60/30/10 vol% $CH_4/CO_2/H_2$). In each case, the fuels are mixed with 50 vol% H_2O.

TABLE I. OCP of ASC operating on various fuels mixed with 50 vol% H_2O.

Fuel Mixture	OCP
Hydrogen (H_2)	0.948 V
Biohydrogen (50/50 vol% H_2/CO_2)	0.925 V
Biogas (60/40 vol% CH_4/CO_2)	1.016 V
Biohythane (60/30/10 vol% $CH_4/CO_2/H_2$)	0.990 V

The output gases of the cell operating on biohythane were measured and characterized by QMS and are shown in Fig. 2 and Table II for a range of oxidant mixtures. Initially, output gases were measured with biohythane mixed with 50/50 vol% H_2O/CO_2 at the OCP. The measurements indicate that 96.7% CH_4 conversion was achieved catalytically, resulting in an output gas mixture composed of 84.8% syngas (H_2 + CO) balanced in CO_2 and 1.3% unconverted CH_4. The syngas was slightly CO-rich, with a H_2/CO ratio of 0.94, suggesting that a mixture of dry reforming [4] and the RWGS reaction [5] were the dominant catalytic processes for this gas mixture. Switching the cell into electrolysis mode increased H_2 production due to electrolysis of unconverted H_2O, increasing the H_2/CO ratio to 1.47. The CO volume decreased causing the total volume of syngas to decrease slightly to 83.7%, although the overall CO_2 and CH_4 conversion stayed approximately constant upon switching to electrolysis mode.

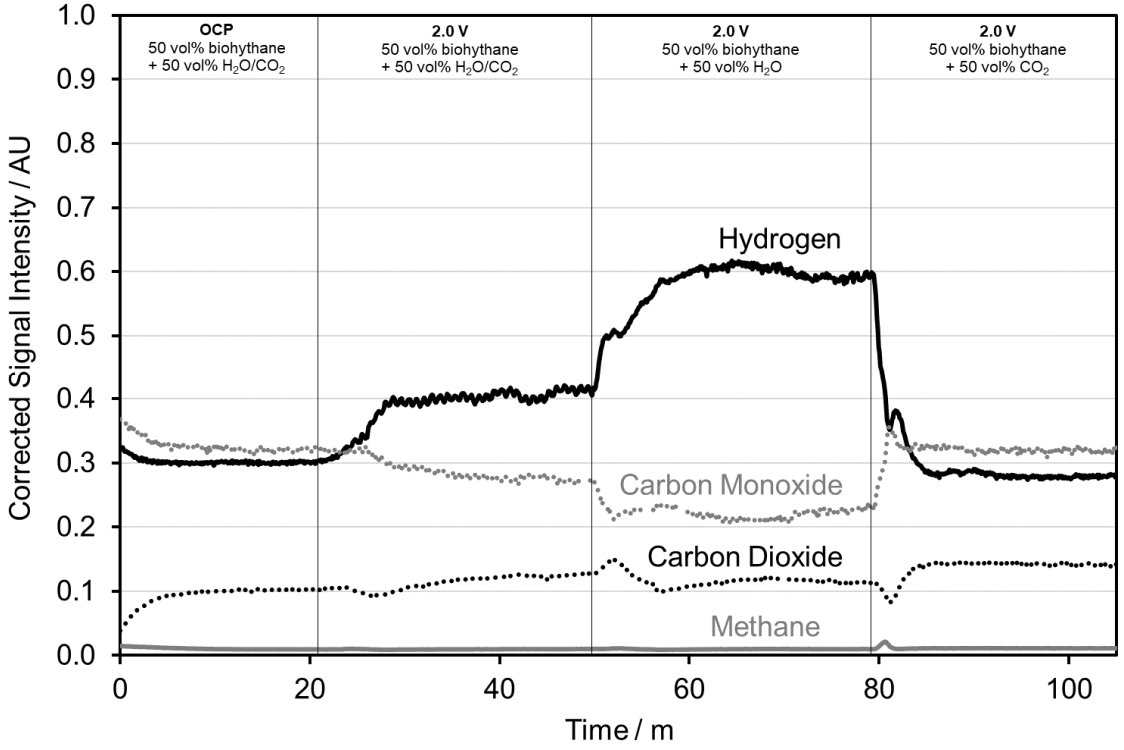

Figure 2. The effect of oxidant composition on the output gases of an ASC operating on biohythane ($CH_4/CO_2/H_2$ 60/30/10 vol%) in electrolysis mode. In each case, biohythane was mixed with 50 vol% of oxidant. The oxidants studied were steam (H_2O), carbon dioxide (CO_2) and a 50/50 vol% H_2O/CO_2 mixture.

TABLE II. Composition and characteristics of output gases shown in Fig. 2. The percentage CH_4 conversion is also provided.

Oxidant Composition	H_2	CO	CH_4	CO_2	Total Syngas	H_2/CO Ratio	CH_4 Conv.
50/50 vol% H_2O/CO_2 (OCP)	41.0%	43.7%	1.3%	13.9%	84.8%	0.94	96.7%
50/50 vol% H_2O/CO_2	49.8%	33.9%	1.2%	15.1%	83.7%	1.47	97.0%
H_2O	63.1%	23.4%	1.1%	12.4%	86.5%	2.69	98.2%
CO_2	37.1%	42.5%	1.5%	19.0%	79.6%	0.87	95.0%

Switching the oxidant to H_2O increased the H_2 content and H_2/CO ratio of the mixture to 2.69, indicating increased electrochemical conversion of H_2O. The CO also decreased due to the decreased presence of CO_2 in the initial mixture. The CH_4 conversion was increased slightly to 98.2%, suggesting that catalytic H_2O reforming was also enhanced by switching to pure H_2O. This mixture gave the highest volume of syngas of 86.5%. The lowest volume of syngas was achieved using pure CO_2, which gave 79.6% syngas and a lower CH_4 conversion of 95.0%. This was because the kinetics of CO_2 conversion catalytically are slower than H_2O conversion.

Further I-V curves and electrochemical impedance spectra were measured to investigate the electrochemical conversion of reactants for the oxidants studied. These are shown in Fig. 3 along with the impedance spectra, which were composed of two polarization arcs: the high frequency arc describes losses associated with surface diffusion and charge transfer (activation losses), the low frequency arc is associated with gas diffusion losses (concentration losses). For each of the co-oxidants, the high frequency arc is 3-5 times larger, indicating the surface diffusion and charge transfer losses dominate. The low frequency arc stayed approximately constant as the co-oxidant was changed, suggesting gas diffusion losses were not greatly influenced by the co-oxidant. The high frequency arc was much more sensitive to co-oxidant, increasing in size as follows: $H_2O < H_2O/CO_2 < CO_2$. The OCP also increased in this order. The data show the performance of the cell was highest when the co-oxidant was H_2O: the OCP was the lowest (0.990 V) and the I-V curve was linear and the impedance arc widths were the narrowest, indicating low activation losses for H_2O.

The I-V curve and EIS data correlate with the observations in Fig. 2. In addition to enhancing catalytic conversion of CH_4, H_2O increased the electrochemical conversion of reactants, since electrochemical conversion and diffusion of H_2O is faster compared with CO_2. This increased H_2 production and therefore led to increased syngas production which was subsequently more H_2-rich. Increasing the use of CO_2 as co-oxidant increased activation losses because CO_2 is more stable and slower to convert than H_2O. Upon switching to H_2O/CO_2 and CO_2, CO_2 did not appear to have a pronounced effect on the gas diffusion losses, but did increase the OCP and the activation losses, reducing the overall kinetic performance of the cell. As well as reducing the H_2/CO ratio and catalytic conversion of CH_4 therefore, using more CO_2 as co-oxidant decreased the overall yield of syngas through electrochemical processes.

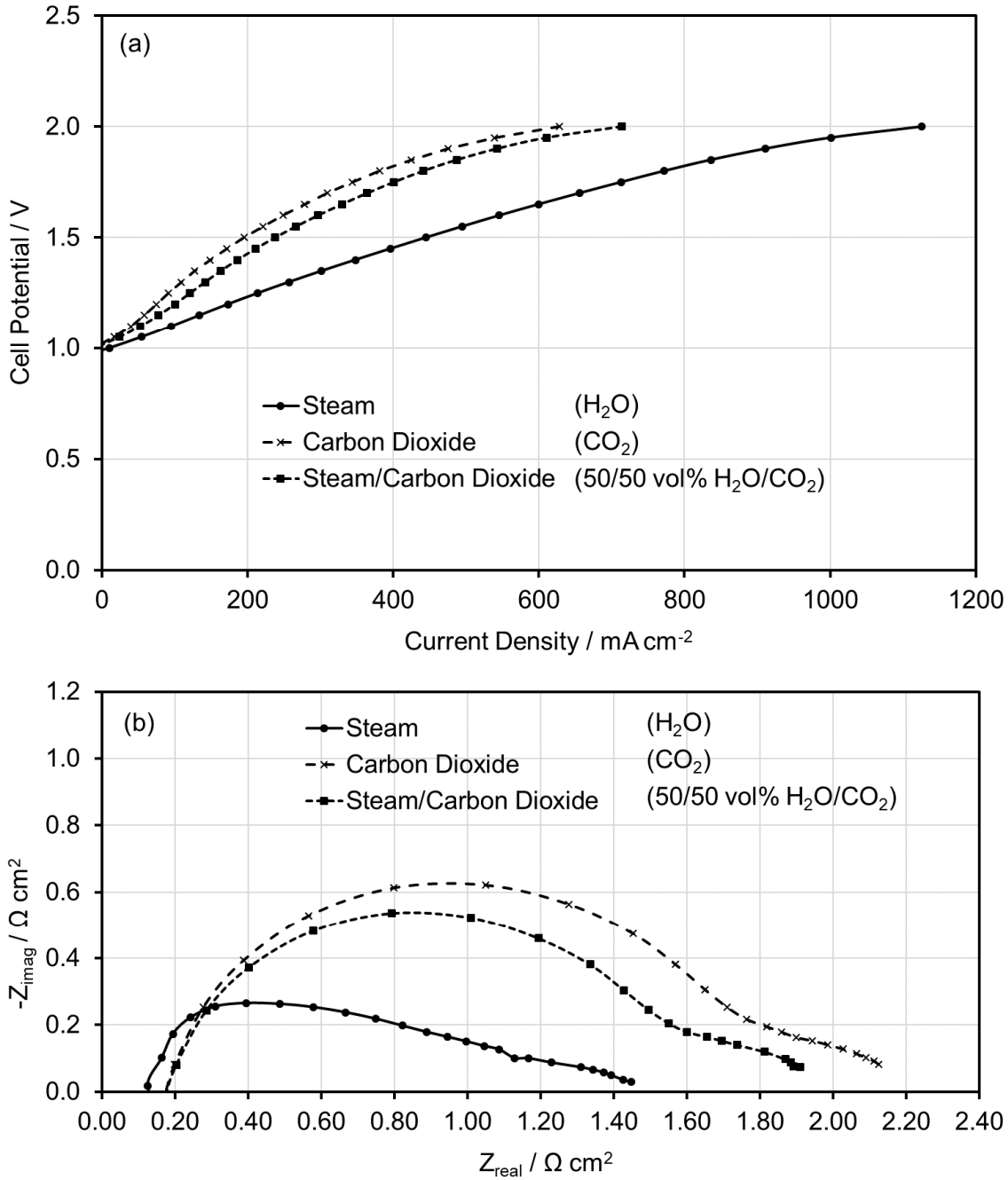

Figure 3. The effect of oxidant composition on the: (a) I-V curve, and (b) electrochemical impedance spectrum, of an ASC operating on biohythane in electrolysis mode.

TABLE III. The effect of oxidant composition on the OCP and EIS arc widths.

Oxidant Composition	OCP	EIS High Frequency Arc Width / Ω cm2	EIS Low Frequency Arc Width / Ω cm2
Steam (H_2O)	0.990 V	1.00	0.32
Carbon Dioxide (CO_2)	1.021 V	1.65	0.31
50/50 vol% H_2O/CO_2	1.015 V	1.43	0.31

Conclusions

This study has investigated co-electrolysis of biohythane using an anode-supported solid oxide fuel cell in electrolysis mode. The work has shown that addition of 10 vol% H_2 to CH_4/CO_2 feedstocks improves the overall performance of the cell compared with H_2-free biogas, which shows considerable performance losses due to anode oxidation and carbon deposition. Cell performance and output gas composition were found to be very dependent on the type of co-oxidant. Using H_2O gave the highest performance, highest syngas yield and highest H_2/CO ratio of all the oxidants. Enhanced performance was due to a mixture of increased catalytic and electrochemical conversion of reactants. The performance decreased in the order $H_2O > H_2O/CO_2 > CO_2$. Increasing the CO_2 decreased both catalytic and electrochemical conversion of reactants and therefore gave lower performance, lower syngas yields and lower H_2/CO ratios.

Acknowledgments

The authors would like to acknowledge the funding provided for this work through the FLEXIS project (C80835). FLEXIS is part-funded by the European Regional Development Fund (ERDF), through the Welsh Government.

References

1. D. Deublein and A. Steinhauser, *Biogas from Waste and Renewable Resources: An Introduction*, p. 49, Wiley-VCH Verlag GmbH & Co. KGaA, Weinheim (2010).
2. B. Bharathirajaa, T. Sudharsanaa, J. Jayamuthunagaib, R. Praveenkumarc, S. Chozhavendhand and J. Iyyappana, *Renew. Sustain. Energy. Rev.*, **90**, 570 (2018).
3. Y. Ren, M. Yu, C. Wu, Q. Wang, M. Gao, Q. Huang and Y. Liu, *Bioresour. Technol.*, **247**, 1069 (2018).
4. J. Bacenettia, C. Sala, A. Fusi and M. Fiala, *Appl. Energy*, **179**, 669 (2016).
5. A. J. Guwy, R. M. Dinsdale, J. R. Kim, J. Massanet-Nicolau and G. Premier, *Bioresour. Technol.*, **102**, 8534 (2011).
6. J. Massanet-Nicolau, R. Dinsdale, A. Guwy and G. Shipley, *Bioresour. Technol.*, **129**, 561 (2013).
7. G. Luo, L. Xie, Q. Zhou and I. Angelidaki, *Bioresour. Technol.*, **102**, 8700 (2011).
8. J. Massanet-Nicolau, R. Dinsdale, A. Guwy and G. Shipley, *Bioresour. Technol.*, **189**, 379 (2015).
9. D. Liu, D. Liu, R. J. Zeng and I. Angelidaki, *Water Res.*, **40**, 2230 (2006).
10. C. Nathao, U. Sirisukpoka and N. Pisutpaisal, *Int. J. Hydrog. Energy*, **38**, 15764 (2013).
11. Z. Chen, L. Bian, L. Wang, N. Chen, H. Zhao, F. Li and K. Chou, *Int. J. Hydrog. Energy*, **41**, 7453 (2016).
12. K. Nikooyeh, R. Clemmer, V. Alzate-Restrepo and J. M. Hill, *Appl. Catal. A*, **347**, 106 (2008).
13. M. J. Escudero, I. Gómez de Parada, A. Fuerte and J. L. Serrano, *J. Power Sources*, **253**, 64 (2014).
14. G. Almutairi, A. Dhir and W. Bujalski, *Fuel Cells*, **14**, 231 (2014).

15. Fiaxell SOFC TechnologiesTM, (2018) https://www.fiaxell.com/
16. C. J. Laycock, K. Panagi, J. P. Reed and A. J. Guwy, *Int. J. Hydrog. Energy*, **43**, 8972 (2018).
17. O. Razbani and M. Assadi, *Int. J. Hydrog. Energy*, **38**, 13781 (2013).
18. B. La Licata, F. Sagnelli, A. Boulanger, A. Lanzini, P. Leone, P. Zitella and M. Santarelli, *Int. J. Hydrog. Energy*, **36**, 7861 (2011).
19. C. J. Laycock, J. Z. Staniforth and R. M. Ormerod, *Dalton Trans.*, **40**, 5494 (2011).
20. J. Staniforth and R. M. Ormerod, *Catal Lett.*, **81**, 19 (2002).
21. K. Kendall, C. M. Finnerty, G. Saunders and J. T. Chung, *J. Power Sources*, **106**, 323 (2002).